THE JOURNAL OF PHYSICAL CHEMISTRY C

ARTICLE

pubs.acs.org/JPCC

Oxygen Binding to Cobalt and Iron Phthalocyanines As Determined from in Situ X-ray Absorption Spectroscopy

Piter S. Miedema,[†] Matti M. van Schooneveld,[†] René Bogerd,[†] Tulio C. R. Rocha,[‡] Michael Hävecker,[§] Axel Knop-Gericke,[‡] and Frank M. F. de Groot*[,†]

[†]Inorganic Chemistry and Catalysis, Department Chemistry, Utrecht University, Universiteitsweg 99, 3584 CG Utrecht, The Netherlands

[‡]Department of Inorganic Chemistry, Fritz-Haber Institut der Max-Planck Gesellschaft, Faradayweg 4-6, 14195 Berlin, Germany

[§]Helmholtz-Zentrum Berlin/Bessy II, Albert-Einstein-Strasse 15, 12489 Berlin, Germany

Supporting Information

ABSTRACT:

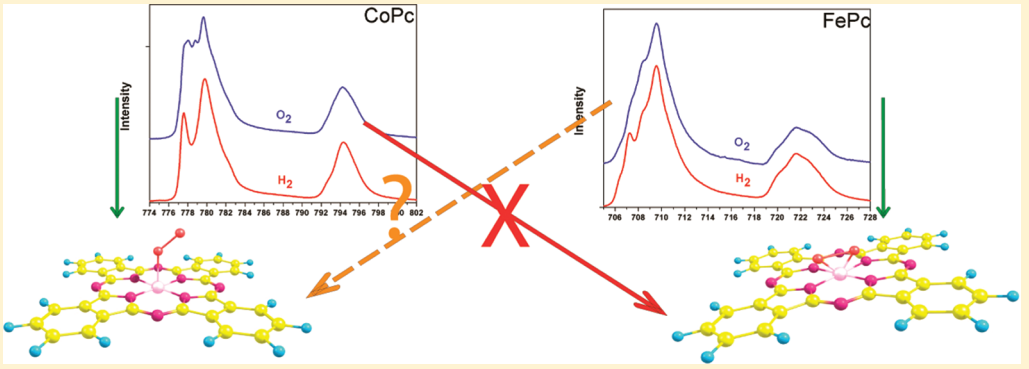

Cobalt phthalocyanine (CoPc) and iron phthalocyanine (FePc) are possible oxygen reduction catalysts in fuel cells, but the exact functioning and deactivation of these catalysts is unknown. The electronic structure of the CoPc and FePc has been studied in situ under hydrogen and oxygen atmospheres by a combination of ambient-pressure X-ray photoelectron spectroscopy and X-ray absorption spectroscopy. The results show that when oxygen is introduced, the iron changes oxidation state while the cobalt does not. The data show that oxygen binds in an end-on configuration in CoPc, while for FePc side-on binding is most likely.

1. INTRODUCTION

The fuel cell converts chemical energy into electrical energy. In case hydrogen is used as the fuel, the only combustion product is water, implying that the technology is as an environmental-friendly alternative for common fuel engines. One of the reasons why the fuel cell is not widely applicable yet is the cost of the cell. For example, for the cathode an expensive platinum catalyst is used. To reduce the costs and improve the performance, studies on platinum alloys are performed.[1,2] Alternatively one can search for a platinum-free cathode catalyst.[3] One option for a platinum-free cathode catalyst is the group of metal phthalocyanines (MPc's, Figure 1).

Already in the 1960s cobalt phthalocyanine (CoPc) was investigated as a fuel cell cathode catalyst.[4] Also iron phthalocyanine (FePc) was studied as catalyst in several oxidation and reduction reactions.[5,6] Experiments have shown that FePc and CoPc exhibit better catalytic performance for catalyzing the cathode reaction than other transition MPc's.[7] The usual cathode half-reaction in the fuel cell, the oxygen reduction reaction (ORR), is

$$O_2 + 4H^+ + 4e^- \rightarrow 2H_2O \quad (1)$$

However, another ORR with oxygen in acidic environment is possible:

$$O_2 + 2H^+ + 2e^- \rightarrow H_2O_2 \quad (2)$$

Different studies have shown that the CoPc catalyst in ORR generates hydrogen peroxide, while the FePc catalyst in ORR generates water and only a small amount of hydrogen peroxide.[6] The FePc and CoPc are still less active than the current platinum catalyst, and, next to that, the MPc's are less stable, with the FePc being more unstable than the CoPc under fuel cell cathode working conditions.[8] To move toward a platinum-free cathode catalyst, it is worthwhile to take a step back and find out how the CoPc and FePc work and how they deactivate. The first step in the catalysis of the ORR is assumed to be the adsorption of the oxygen molecule on the central metal atom of the MPc. Electrons are withdrawn from the catalyst to the adsorbed O_2, followed by ORR to form either H_2O or H_2O_2.

Received: September 26, 2011
Revised: November 10, 2011
Published: November 17, 2011

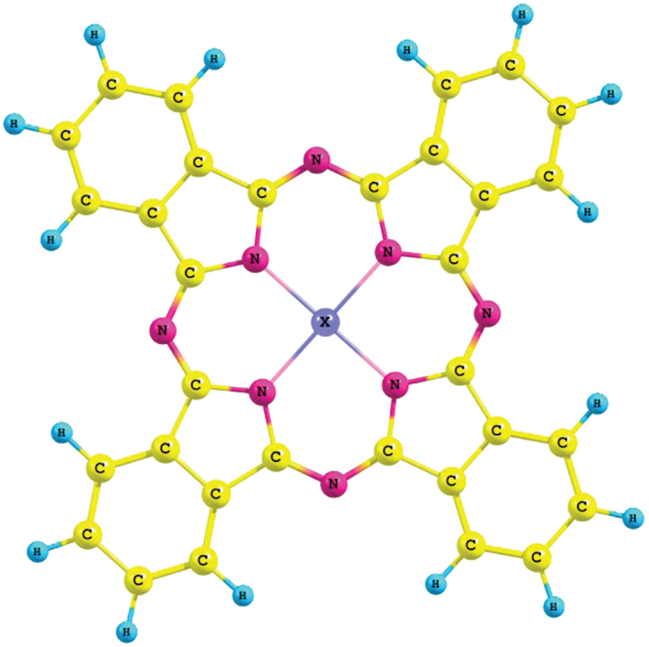

Figure 1. Structure formula of metal phthalocyanines, where X is a metal atom.

The main two possible fashions for O_2 to be adsorbed on MPćs are the end-on configuration (Pauling's model[9]) and the side-on configuration (Griffith's model[10]).

In an end-on configuration, one oxygen atom is right above the central atom over the catalyst molecule plane and the other oxygen atom is farther away from the metal atom with a Fe−O−O angle of approximately 120° (Figure 2, top panel).[9]

In a side-on configuration the adsorbed O_2 molecule extends parallel to the catalyst molecule plane and the two oxygen atoms are in equal distance from the central metal atom (Figure 2, bottom panel). In the side-on configuration there is often electronic transfer from the metal to the oxygen atoms (metal to ligand charge transfer). For both the end-on and side-on configuration there are two options: (a) with the oxygen directly above an M−N bond and (b) with the oxygen atoms above the space between two M−N bonds. Density functional theory (DFT) studies with the PW91 exchange-correlation potential and a double numeric basis with polarization functions as basis sets, on the oxygen bonding to CoPc and FePc by Wang et al.,[11] showed that for FePc both the side-on and end-on structures with O_2 are stable, with the end-on structure being more stable with about 0.7 eV. The DFT calculations of O_2 adsorbed on CoPc by Wang et al. showed that only the end-on configurations are energetically stable. It is strongly suggested that the O−O bonds in the adsorbed O_2 molecules were much weaker in the side-on configuration than in the end-on configurations. The weakening of the bonds makes the adsorbed O_2 molecules in side-on configurations more active in participating in ORR. From their DFT calculations, Wang et al. propose that FePc can promote four-electron ORR, because side-on O_2 adsorption is energetically permitted. In contrast, because only end-on O_2 adsorption is possible on CoPc, Wang et al. state that this is the reason why only two-electron ORR can occur on CoPc. The reason for this is that, in the end-on O_2 adsorption configurations, the O atom which is closer to the transition metal atom gets much less transferred charge from the catalyst molecules than the other O atom. This may allow the

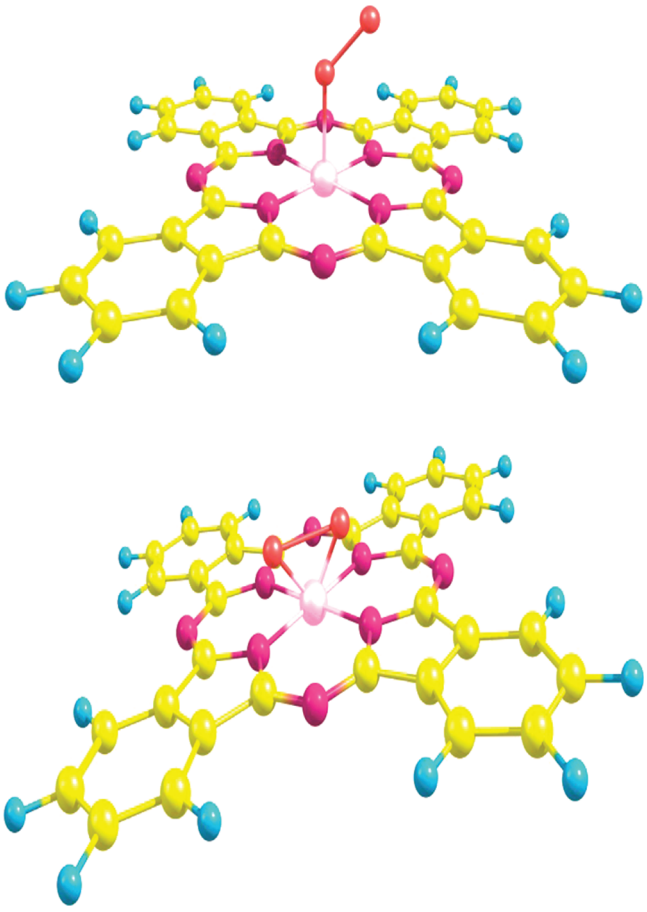

Figure 2. Top panel: oxygen binding to MPc in an end-on configuration. Bottom panel: oxygen binding to MPc in a side-on configuration.

O atom that is farther away from the transition metal atom to react first to form peroxide via a two-electron reduction. In the side-on O_2 adsorption configurations, the two O atoms have equal distance to the transition metal atom and are equally charged. Thus, it is possible that the ORR takes place at the same time on the two O atoms and proceeds via a four-electron process and the side-on adsorbed O_2 would determine the main characteristics of ORR even though the end-on adsorbed O_2 are energetically more stable. All the propositions by Wang et al. were solely based on their DFT calculations.

In this study we carry out a set of experiments in order to get further insights into these systems and to check the aforementioned theoretical predictions.[11] In situ L-edge X-ray photoelectron (XPS) and X-ray absorption spectroscopy (XAS) measurements are performed on the CoPc and FePc in both oxygen and hydrogen environments. Note that both FePc and CoPc are not in realistic fuel-cell conditions, such as in an acid environment. However, in the ORR the rate determining step is assumed to be the electron transfer between the catalyst and the oxygen[6,12] and the main event for this rate determining step is the oxygen adsorption,[8] which means that in this study we look at (part of) the rate determining step of the ORR. To understand the Co and Fe $L_{2,3}$-edge XAS in detail with all its features, crystal field multiplet calculations are performed. A major challenge in these calculations is that the electronic structure of the central Fe atom in FePc is unclear. The Fe^{2+} could be either in a high-, intermediate-, or low-spin state, and in addition the 3d-orbital occupation

dx.doi.org/10.1021/jp209295f |J. Phys. Chem. C 2011, 115, 25422–25428

has to be decided. In recent literature, the agreement is that the iron center is in the intermediate-spin state,[13−17] but the discussion is undecided whether it is a $^3A_2$, $^3B_2$, or ^3E state. Recent combinations of experiments and calculations have shown that the Fe^{2+} is most likely in the ^3E spin state.[16,18] Taking the ^3E as ground state, semiempirical multiplet calculations on the Fe $L_{2,3}$-edge XAS were performed using spin-state phase diagrams as starting point. It is known that the XAS shape depends on the spin state, which in turn depends on the chosen crystal field parameters. Measured in situ Fe 2p XPS are compared with charge-transfer multiplet calculations. The in situ nitrogen K-edge XAS are compared with time-dependent density functional theory (TDDFT) calculations. The Fe 2p XPS and nitrogen K-edge XAS[19] complement the results of the metal $L_{2,3}$-edge XAS.

2. EXPERIMENTAL AND COMPUTATIONAL DETAILS

2.1. In Situ XAS and XPS Experiments. $Co^{II}Pc$ powder, 97% from Aldrich, and $Fe^{II}Pc$ powder, 96% from Alfa Aesar, as received were pelletized. The electronic structure of the CoPc and FePc pellets was studied in situ using XAS and XPS.[20−22] Experiments were performed at the ISISS-PGM beamline at the Berliner Synchrotron Radiation Facility (BESSY) in Berlin (Germany). The experimental setup and principles for measuring in situ XAS and XPS are described in more detail elsewhere.[23−26] In brief, the samples were pressed into a self-supporting wafer (∼20 mg) and mounted on a sapphire sample holder, 2 mm away from a 1 mm diameter aperture to a differentially pumped electrostatic lens system. XAS measurements at the Fe $L_{2,3}$-, Co $L_{2,3}$-, N K-, and O K-edge are performed using gas-phase conversion electron yield (CEY) detection.[25] The resolution of the XAS measurements was ∼0.1 eV at the Co and Fe $L_{2,3}$-edge. In situ Fe 2p XPS measurements have been performed using incident X-ray energy of 1215 eV. The XPS peak positions were calibrated with respect to the main C 1s XPS peak (284.7 eV) or to the Fermi energy. The energy calibration by carbon was confirmed by the Fermi energy calibration; however, due to low signal-to-noise ratio in the Fermi energy, limiting the calibration accuracy, the Fermi energy calibration was not used as the main correction. All XAS and XPS measurements were performed at room temperature. Gas flows of H_2 or O_2 through the reaction cell, leading to 0.5 mbar pressure in the cell, were regulated through mass flow controllers.

2.2. Crystal Field Multiplet Calculations. Experimental XAS are compared with crystal field multiplet calculations[27,28] using the CTM4XAS interface.[29] This approach includes both electron−electron interactions and spin−orbit coupling for each open subshell of one atom. For simulation of the spectra, Slater−Condon parameters are used. Atomic Slater−Condon parameters can be approximated by 80% of the Hartree−Fock calculated values.[30] The Fe and Co $L_{2,3}$ spectra are calculated from the sum of all possible transitions for an electron excited from the 2p core level into an unoccupied 3d level. The ground state is approximated by the electronic configuration $3d^n$. In the ground state, 3d spin−orbit coupling and the crystal field affect the $3d^n$ configuration. The $3d^n$ ground state and the $2p^53d^{n+1}$ final state are affected by the 3d3d multiplet coupling. In the final state also the 2p3d multiplet coupling, the 2p and 3d spin−orbit couplings, and the crystal field potential in D_{4h} symmetry are included. The strength of the crystal field is described with empirical parameters 10Dq, Ds, and Dt, and those are optimized to experiment.[27] The calculations provide the excitations and their oscillator strengths. These stick spectra are broadened with both a Lorentzian and Gaussian broadening to simulate the lifetime broadening and the experimental resolution, respectively. In this research the L_3- and L_2-edges were broadened with a Lorentzian of 0.3 and 0.4 eV, respectively, and additionally with a Gaussian of 0.2 eV. For XPS simulations, extra parameters for the charge transfer (Δ, U, Q, and Tt_{2g} and Te_g) have to be included in the multiplet calculations. Multiplet calculations have been performed before on both XAS of FePc and CoPc under vacuum.[16,18,31] The crystal field parameters in those studies are the starting point in our fitting procedure.

2.3. TDDFT Calculations. All DFT calculations are performed using the ORCA program package.[32,33] Geometry optimization of these molecules was performed using the BP86 potential and TZV-ZORA basis set for the metal atom and SV-ZORA basis sets[34] for the other atoms, and the Ahlrichs (2df,2pd) polarization functions were obtained from the TurboMole basis set library under ftp.chemie.unikarlsruhe.de/pub/basen.[35,36] Subsequently the new geometry was optimized with the B3LYP potential TZV-ZORA basis set for the metal and SV-ZORA basis sets for the other atoms. All of the geometry optimizations achieved convergence within 50 cycles. The difference between the first and second geometry optimization step was negligible. Oxygen molecules are attached to the metal of the optimized FePc and CoPc molecules in four geometries as reported by Wang et al.,[11] and then the distances of the O_2 to MPc are optimized using BP86, only the first geometry optimization step as mentioned above. The molecules named O_2-MPc_opt1 and O_2-MPc_opt2 represent O_2 adsorbed in an end-on configuration to metal M and O_2-MPc_opt3 and O_2_MPc_opt4 represent O_2 adsorbed in a side-on configuration to metal M, where M = Fe, Co. Our DFT calculations agree with Wang et al. that the CoPc with O_2 in side-on configurations have negative adsorption energies and are therefore not stable, while the FePc has positive adsorption energies for both O_2 in the side-on and end-on configurations.

Following the ground-state DFT geometry optimization, TD DFT calculations were performed, allowing only excitations from the N 1s orbitals. The TDDFT approach in ORCA that was used is a linear response including the Tamm−Dancoff approximation (TDA). The XAS of the optimized molecules are calculated with the TDDFT package in the ORCA program[37−41] using the CP(PPP) basis set[42] for the metal and TZVP basis set for all other atoms with zero-order relativistic approximation (TZV-ZORA).[34]

3. RESULTS

The results section is split into four parts; we discuss respectively in section 3.1 the Co $L_{2,3}$-edge XAS, in section 3.2 the Fe $L_{2,3}$-edge XAS, in section 3.3 the Fe 2p XPS, and in section 3.4 the nitrogen K-edge XAS.

3.1. Co $L_{2,3}$-Edge XAS of CoPc. The experimental Co $L_{2,3}$-edge XAS for a CoPc pellet are shown in Figure 3. These XAS were taken after no changes in the Co $L_{2,3}$-edge and N K-edge XAS in the new gas environment were noticed anymore. The XAS of CoPc in helium (black) and in the first cycle of hydrogen (red) resemble each other. The XAS of CoPc in oxygen (blue) is drastically different at the L_3-edge. After being in contact with O_2, the Co $L_{2,3}$-edge XAS does not seem to change in the reducing H_2 environment (H_2(2nd), red). The XAS also does not change in the CO environment (Supporting Information, section SI.1).

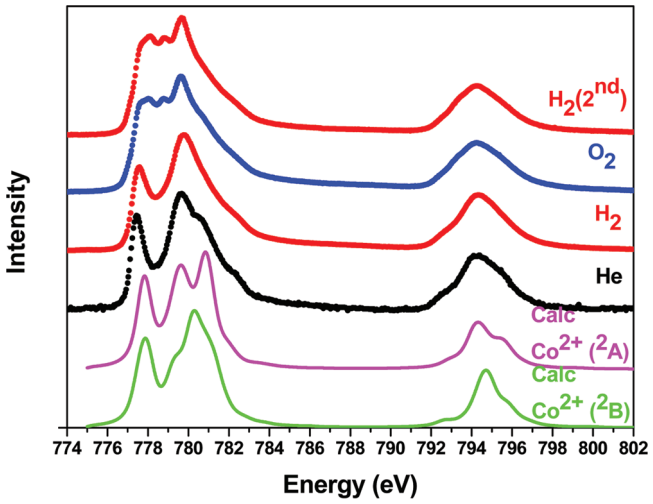

Figure 3. Co $L_{2,3}$-edge XAS, from bottom to top, a multiplet calculation of Co^{2+} with 10Dq = 2.3, Dt = 0.2, and Ds = 0.7 eV (green, ^2B), a multiplet calculation of Co^{2+} with 10Dq = 2.3, Dt = 0.2, and Ds = 0.5 eV (pink ^2A), experimental spectra of CoPc pellet in helium (He, black), hydrogen (H_2, red), oxygen (O_2, blue) and for the second time in hydrogen (H_2(2nd), red) environment with gas pressures of 0.5 mbar.

Co $L_{2,3}$-edge XAS were calculated with crystal field multiplet theory using the CTM4XAS interface[29] and are compared to the experimental spectra in the same figure (Figure 3).

The Co $L_{2,3}$-edge XAS of CoPc in H_2 has agreement with the XAS of a crystal field multiplet calculation of Co^{2+} with crystal field parameters 10Dq = 2.3, Dt = 0.2, and Ds = 0.7 eV and Slater integrals reduced to 75% of the atomic values. With these parameters, the energy difference between the t_{2g} and e_g (in O_h symmetry) is $\Delta_0 = 1.13$ eV. The ground state of the Co^{2+} in this symmetry and crystal field is low-spin ^2B ($d_{xz,yz}^4 d_{z^2}^2 d_{xy}^1$). The XAS shape of CoPc in H_2 is reproduced by the calculation. Covalent effects are not fully taken into account in the present multiplet calculation. Extended Slater integral reduction, meaning lower than 80% of the Hartree−Fock values, can give a first approximation to covalent effects, as used here.

The Co $L_{2,3}$-edge of CoPc in O_2 is in close agreement with a multiplet calculation of Co^{2+} using crystal field parameters 10Dq = 2.3, Dt = 0.2, and Ds = 0.5 eV and Slater integrals again reduced to 75% of the atomic values. With these parameters, the energy difference between the t_{2g} and e_g (in O_h symmetry) is $\Delta_0 = 1.13$ eV. Only the Ds value is lower in comparison with the multiplet calculation for CoPc in H_2 mentioned above. This agrees with the expectation that O_2 bound to CoPc makes the symmetry around the Co atom more "octahedral-like", so the Ds value should become smaller. With the lower Ds value the occupation of the 3d orbitals changes such that the ground state of Co^{2+} in this crystal field is low-spin ^2A ($d_{xz,yz}^4 d_{xy}^2 d_{z^2}^1$). In the case of CoPc in O_2, the values for the crystal field agree much better with recently published multiplet calculations for CoPc films.[18] O_2 has an effect on CoPc that leads to crystal field similar to those of ordered multilayer CoPc films. This shows that the ground state of the Co^{2+} in CoPc is delicate. Small perturbations change the 3d-orbital occupation and therefore the symmetry state. We performed multiplet calculations with Co^{3+}, but these did not agree with the experimental XAS of CoPc in H_2 or in O_2. This led to the conclusion that the Co ion in CoPc is low-spin Co^{2+} in all gas environments measured (^2B symmetry in H_2 and ^2A in O_2). The electronic configuration of cobalt is stable after 0.5 mbar of oxygen has been in contact with CoPc.

3.2. Fe $L_{2,3}$-Edge XAS of FePc. The experimental Fe $L_{2,3}$-edge XAS for a FePc pellet under vacuum and under 0.5 mbar pressure of respectively O_2, H_2, and a second cycle of O_2 are shown in Figure 4. These XAS were taken right after the moment at which no changes in the Fe 2p and N 1s XPS spectra in the new gas environment were observed anymore.

The XAS pattern of FePc in O_2 (blue), compared to the XAS of FePc under vacuum (black), changes at the L_3-edge, resulting in only a main peak at the higher energy side. For FePc in H_2 (red) after being in O_2 atmosphere the XAS only slightly differs from the Fe $L_{2,3}$-edge XAS of FePc in vacuum (black), so the XAS returns to the XAS of FePc at the start. The XAS of FePc in the second cycle of O_2 resembles again the FePc in the first cycle of O_2.

The XAS of FePc under vacuum and the FePc in O_2 are compared with multiplet calculations of Fe^{2+} with 10Dq = 2.7, Ds = 0.86, and Dt = 0.247 eV ($\Delta_0 = 1.26$ eV) and Fe^{3+} with 10Dq = 1.8 and Ds = Dt = 0 eV ($\Delta_0 = 1.80$ eV). Atomic Slater integrals were used. The ground states of Fe^{2+} and Fe^{3+} are ^3E ($d_{xz,yz}^3 d_{xy}^2 d_{z2}^1$, and $^6A_1$ ($d_{xz,yz}^2 d_{xy}^1 d_{z^2}^1 d_{x^2-y^2}^1$), respectively. This implies that Fe^{2+} is in an intermediate-spin (IS) state as suggested for FePc.[13−17] In contrast Fe^{3+} is in a high-spin (HS) state.

The XAS of FePc under vacuum agrees with XAS of the Fe^{2+} multiplet calculation with an intermediate-spin ground state as can be seen in Figure 4. The L_3 pattern is especially reproduced by the Fe^{2+} calculation. We cannot exclude that there is some small contribution of Fe^{3+} high spin in the experimental spectrum of FePc under vacuum.

The XAS of FePc in O_2 has resemblance to the multiplet calculation of Fe^{3+} high spin (Figure 4). The XAS of FePc in oxygen contains more Fe^{3+} contribution than the XAS of FePc under vacuum. We conclude that the sample is a mixture of approximately 30 ± 10% of Fe^{2+} IS and 70 ± 10% Fe^{3+} HS.

The total integrated area of the $L_{2,3}$-edge gives direct information about the amount of holes present and therefore about the relative oxidation state of the metal. Second, there is a relationship between the branching ratio $L_3/(L_2 + L_3)$ and the spin state.[43,44] The integrated areas of some spectra are shown in Table 1. In this analysis, we assume that the L_3-edge ends and L_2-edge starts at 717 eV for FePc and at 788 for CoPc. The integrated areas support that the Fe ion changes partially from Fe^{2+} to Fe^{3+} going from H_2 to O_2 environment, since the total area for FePc in H_2 is 0.148 and it becomes higher for FePc in O_2, suggesting an increase in the amount of 3d holes and therefore a partial change from Fe^{2+} (d^6) to Fe^{3+} (d^5). The total integrated area for CoPc in H_2 and O_2 is constant, confirming that there is no oxidation state change for the Co ion going from CoPc in H_2 to CoPc in O_2. The branching ratio confirms that there is a spin-state change between FePc in H_2 and FePc in O_2, while the difference between the branching ratio of CoPc in H_2 and CoPc in O_2 is less significant, supporting the observation that the Co does not change spin state; only the electrons are redistributed in other d orbitals. One would expect that the total area, that is related to the d holes, would be higher for Fe^{2+} and Fe^{3+} than for Co^{2+}, since Co^{2+}, Fe^{2+}, and Fe^{3+} have three, four, and five d holes, respectively. However, that is not the case here. The differences can be ascribed to the different background of the un-normalized XAS for the different samples FePc and CoPc, so only relative differences between CoPc in H_2 and O_2 on one side and between FePc in H_2 and O_2 on the other side give useful information.

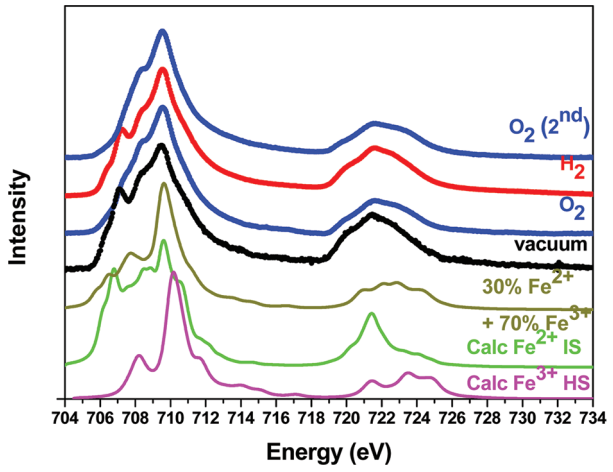

Figure 4. Fe $L_{2,3}$-edge XAS, from bottom to top, a multiplet calculation of Fe^{3+} with 10Dq = 1.8, Ds = Dt = 0 eV (pink, calcd Fe^{3+} HS), a multiplet calculation of Fe^{2+} with 10Dq = 2.7, Ds = 0.86, and Dt = 0.247 eV (green, calcd Fe^{2+} IS) and of a combination of the multiplet calculations with 30% Fe^{2+} and 70% Fe^{3+}, experimental spectra (dark yellow, 30% Fe^{2+} + 70% Fe^{3+}) of FePc in vacuum (black), oxygen (blue), in hydrogen (H_2, red), and for the second time in oxygen (O_2(2nd), blue) environment with gas pressures of 0.5 mbar.

Table 1. Integrated Total, L_3 and L_2 Area of the Fe or Co $L_{2,3}$-edge of XAS Spectra in H_2 and O_2 Only Normalized to the Ring Current

spectrum	total area	area L_3	area L_2	$L_3/(L_2 + L_3)$
FePc in H_2	0.148	0.102	0.046	0.688
FePc in O_2	0.162	0.128	0.034	0.788
CoPc in H_2	0.177	0.123	0.054	0.695
CoPc in O_2	0.179	0.129	0.050	0.719

3.3. Iron 2p XPS. The partial change of the Fe oxidation state from H_2 to O_2 is also visible in the 2p photoelectron spectra measured under the same conditions, just before the absorption spectra, as given in the Supporting Information section SI.3.

3.4. Nitrogen K-Edges. The nitrogen (N) K-edge XAS were studied in different gas environments. For more information about N K-edge XAS of transition metal systems we refer to Chen et al.[19] The measured data were corrected for the absorption of the Si_3N_4 membranes. The procedure is mentioned in the Supporting Information, section SI.4. The results are presented for CoPc and FePc. XAS of the oxygen K-edge are given in the Supporting Information, sections SI.9 and SI.10. In the following figures the experimental N K-edge of CoPc in H_2 and O_2 and FePc in H_2 are shown. In Figure 5 the N K-edge XAS is shown. The N K-edge XAS of CoPc in H_2 after O_2 introduction shows changes in the intensity at 397 eV (peak C, a small difference between black and green lines) and 399.7 eV (peak D), which we ascribe to changes in the nitrogen atoms surrounding the Co ion that supply charge to the O_2 bonding. Note that in these N K-edge spectra some N_2 gas is observed (as compared with the Au foil in N_2, peaks between 400 and 402 eV), which means there was a N_2 leak.

The N K-edge XAS of FePc in H_2 (red line) and of FePc in the second cycle of H_2 (green line) in Figure 6 show that the N K-edge changes slightly in O_2 with respect to H_2. The N K-edge XAS of FePc in O_2 are not shown here (see Supporting Information section SI.5), but it only shows some tiny deviations with the N K-edge spectra in H_2. The nitrogen atoms in the FePc do not seem to contribute significant charge to the oxygen binding. There are no differences between the N K-edge of FePc in H_2 before and after O_2 introduction. Combined with the similar Fe L-edge XAS of FePc under vacuum and H_2 after O_2 introduction, this suggests that the O_2 or the fragments of O_2 are more easily released from the FePc than from the CoPc.

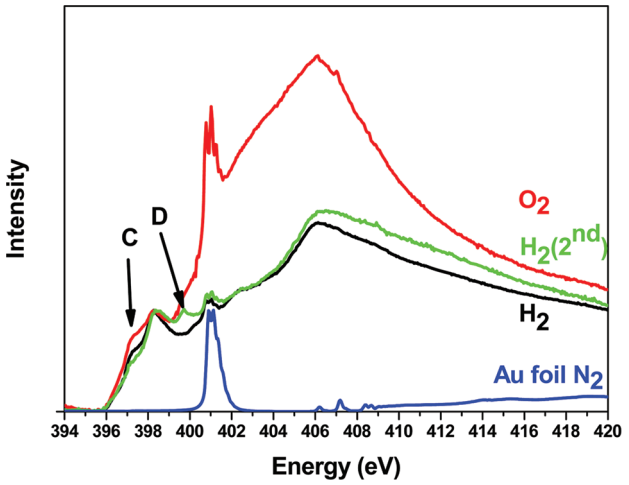

Figure 5. In situ N K-edge XAS of CoPc in H_2 (black), O_2 (red), and in the second cycle of H_2 after O_2 introduction (green) environment with gas pressures of 0.5 mbar. An Au foil reference in N_2 (blue) is shown for comparison for the peaks in the 400−402 eV energy range.

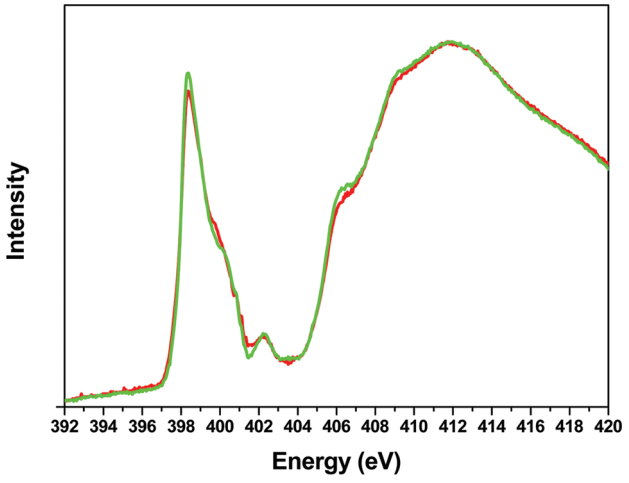

Figure 6. In situ N K-edge XAS of FePc in H_2 (red) and of FePc in the second cycle of H_2 (green) environment with gas pressures of 0.5 mbar.

4. DISCUSSION

The oxidation-state change for the Fe between H_2 and O_2, also found by Cook et al. for FePc in air[45] and the lack of oxidation-state change for the Co, illustrates that CoPc and FePc have different ways of oxygen adsorption. Wang et al. mention that there is more charge transfer from the MPc molecules to the absorbed O_2 molecules in the side-on configurations than the end-on configurations, on the basis of Mullikan charge analysis. This suggests that the experimentally obtained oxidation-state

change of Fe between H_2 and O_2 indicates that the O_2 binds in a side-on configuration to FePc, as previously found by calculations from Wang et al.[11] However, for FePc in O_2, peaks indicative for Fe^{2+} are still visible in both the Fe $L_{2,3}$-edge XAS and Fe 2p XPS. Most likely the remaining Fe^{2+} in the O_2 environment is related to the FePc that is not in direct contact with the O_2 gas. Part of the FePc that is not in direct contact with the O_2 gas is taken into account in the measurement of CEY-XAS and XPS measurements, implying that one observes Fe^{2+} which is not directly in contact with O_2 plus surface Fe^{3+}. Alternatively, this Fe^{2+} could indicate that there is a small part of O_2 bound in the end-on configuration. Wang et al.[11] and Sabelli and Melendres[46] found that the end-on configuration for O_2 bound to FePc (without oxidation-state change) is more stable than the side-on configuration, so bonding of O_2 to FePc in an end-on configuration might also be a possible explanation for the remaining Fe^{2+} in O_2. For the CoPc, the Co ion remains Co^{2+}, which means that there is no side-on O_2 configuration on CoPc and only end-on configuration is allowed as expected.

Comparing the experimental data with XAS calculations reveals that multiplet calculations using CTM4XAS can capture the main features in the XAS and XPS and provide valuable insights for the peak assignments and interpretation of spectral changes, but the disadvantage is that one has to fit several semiempirical parameters for lower symmetry compounds.

The N K-edge XAS of CoPc in H_2 and O_2 show that the nitrogen atoms (surrounding the Co) contribute in some way to the O_2 adsorption, while the N K-edge XAS of FePc in H_2 before and after O_2 introduction show that there is a negligible effect of the nitrogen atoms (surrounding the Fe) to the O_2 adsorption to FePc.

5. CONCLUSIONS

The Co $L_{2,3}$-edge XAS as interpreted by crystal field and charge-transfer multiplet calculations show that Co in CoPc is in the low-spin state. In oxygen atmosphere, the occupation of the 3d orbitals changes and the symmetry changes from ^{2}B to ^{2}A, but the spin state remains low-spin. After the CoPc has been in contact with O_2, the 3d-orbital occupation remains fixed; i.e., the symmetry remains ^{2}A. This can be due to the strong bonding of oxygen to CoPc or to the tendency that ^{2}A is the preferred low-spin state over ^{2}B in more octahedral-like surrounding.

The Fe $L_{2,3}$-edge XAS combined with the multiplet calculations show that Fe in FePc under vacuum is in the ^{3}E intermediate-spin state. In O_2, the Fe oxidation state shifts to high-spin Fe^{3+}, indicating a charge transfer from the metal to the oxygen in oxygen binding. Since the Co does not change oxidation state in O_2 compared to H_2, the O_2 binding is likely to happen in the end-on configuration. This agrees well with the DFT calculations by Wang et al.[11] and thereby provides experimental data supporting the proposition of the binding model with an expected half-reaction for the ORR.

■ ASSOCIATED CONTENT

Supporting Information. Figures showing Co L-edge XAS of CoPc in CO, Fe L-edge XAS of FePc in CO, Fe 2p XPS of FePc in H_2 and O_2 and with use of CTM4XAS interface for Fe^{2+}, raw N K-edge XAS of CoPc, N K-edge of a cleaned Au foil, N K-edge XAS of FePc in O_2, and TDDFT calculations on various CoPc configurations, the N K-edge XAS of CoPc and O_2-CoPc and a zoomed in focus of the region between 394 and 402 eV, the N K-edge of FePc configurations, the O K-edge of CoPc, and the O K-edge XAS of FePc, text describing Co L-edge XAS of CoPc in CO, Fe L-edge XAS of FePc in CO, Fe 2p XPS of FePc in H_2 and O_2, raw N K-edge XAS of CoPc, and (TD)DFT calculations on O_2−FePc and O_2−CoPc and in situ O K-edge XAS of FePc and CoPc, and tables listing geometries of FePc and CoPc and spin state 2S + 1 with the single-point energy and absorption geometry and spin state results. This material is available free of charge via the Internet at http://pubs.acs.org.

■ AUTHOR INFORMATION

Corresponding Author
*E-mail: f.m.f.degroot@uu.nl.

■ ACKNOWLEDGMENT

The Helmholtz-Zentrum Berlin−Electron storage ring BESSY II is acknowledged for provision of synchrotron radiation at beamline ISIS-PGM. The research leading to these results has received funding from the European Community's Seventh Framework Programme (FP7/2007-2013) under grant agreement no. 226716. PSM, MMvS and FMFdG acknowledge NWO−CW/VICI for funding.

■ REFERENCES

(1) Bing, Y.; Liu, H.; Zhang, L.; Ghosh, D.; Zhang, J. *Chem. Soc. Rev.* **2010**, *39*, 2184–2202.
(2) Mani, P.; Srivastava, R.; Strasser, P. *J. Power Sources* **2011**, *196*, 666–673.
(3) Bambagioni, V.; Bianchini, C.; Filippi, J.; Lavacchi, A.; Oberhauser, W.; Marchionni, A.; Moneti, S.; Vizza, F.; Psaro, R.; Dal Santo, V.; Gallo, A.; Recchia, S.; Sordelli, L. *J. Power Sources* **2011**, *196*, 2519–2529.
(4) Jasinski, R. *J. Electrochem. Soc.* **1965**, *112*, 526–528.
(5) Jasinski, R. *Nature* **1964**, *201*, 1212–1213.
(6) Zagal, J. H. *Coord. Chem. Rev.* **1992**, *119*, 89–136.
(7) van Veen, J. A. R.; Visser, C. *Electrochim. Acta* **1979**, *24*, 921–928.
(8) Chen, R.; Li, H.; Chu, D.; Wang, G. *J. Phys. Chem. C* **2009**, *113*, 20689–20697.
(9) Pauling, L. *Nature* **1964**, *203*, 182–183.
(10) Griffith, J. S. *Proc. R. Soc. London, Ser. A* **1956**, *235*, 23–36.
(11) Wang, G.; Ramesh, N.; Hsu, A.; Chu, D.; Chen, R. *Mol. Simul.* **2008**, *34*, 1051–1056.
(12) Randin, J.-P. *Electrochim. Acta* **1974**, *19*, 83–85.
(13) Åhlund, J.; Nilson, K.; Schiessling, J.; Kjeldgaard, L.; Berner, S.; Mårtensson, N.; Puglia, C.; Brena, B.; Nyberg, M.; Luo, Y. *J. Chem. Phys.* **2006**, *125*, 034709.
(14) Barraclough, C. G.; Martin, R. L.; Mitra, S.; Sherwood, R. C. *J. Chem. Phys.* **1970**, *53*, 1643–1648.
(15) Liao, M. -.; Scheiner, S. *J. Chem. Phys.* **2001**, *114*, 9780–9791.
(16) Miedema, P. S.; Stepanow, S.; Gambardella, P.; De Groot, F. M. F. *J. Phys.: Conf. Ser.* **2009**, 190.
(17) Reynolds, P. A.; Figgis, B. N. *Inorg. Chem.* **1991**, *30*, 2294–2300.
(18) Stepanow, S.; Miedema, P. S.; Mugarza, A.; Ceballos, G.; Moras, P.; Cezar, J. C.; Carbone, C.; de Groot, F. M. F.; Gambardella, P. *Phys. Rev. B* **2011**, *83*, No. 220401.
(19) Chen, J. G. *Surf. Sci. Rep.* **1997**, *30*, 1–152.
(20) Heijboer, W. M.; Battiston, A. A.; Knop-Gericke, A.; Hävecker, M.; Bluhm, H.; Weckhuysen, B. M.; Koningsberger, D. C.; De Groot, F. M. F. *Phys. Chem. Chem. Phys.* **2003**, *5*, 4484–4491.
(21) Heijboer, W. M.; Battiston, A. A.; Knop-Gericke, A.; Hävecker, M.; Mayer, R.; Bluhm, H.; Schlögl, R.; Weckhuysen, B. M.; Koningsberger, D. C.; De Groot, F. M. F. *J. Phys. Chem. B* **2003**, *107*, 13069–13075.

(22) de Smit, E.; van Schooneveld, M. M.; Cinquini, F.; Bluhm, H.; Sautet, P.; de Groot, F. M. F.; Weckhuysen, B. M. On the Surface Chemistry of Iron Oxides in Reactive Gas Atmospheres. *Angew. Chem., Int. Ed.* **2011**, *50*, 1584–1588.
(23) Bluhm, H.; Hävecker, M.; Knop-Gericke, A.; Kleimenov, E.; Schlbögl, R.; Teschner, D.; Bukhtiyarov, V. I.; Ogletree, D. F.; Salmeron, M. *J. Phys. Chem. B* **2004**, *108*, 14340–14347.
(24) Bluhm, H.; Hävecker, M.; Knop-Gericke, A.; Kiskinova, M.; Schlögl, R.; Salmeron, M. *MRS Bull.* **2007**, *32*, 1022–1030.
(25) Knop-Gericke, A.; Hävecker, M.; Neisius, T.; Schedel-Niedrig, T. *Nucl. Instrum. Methods Phys. Res., Sect. A* **1998**, *406*, 311–322.
(26) Knop-Gericke, A.; Havecker, M.; Schedel-Niedrig, T.; Schlogl, R. *Top. Catal.* **2000**, *10*, 187–198.
(27) de Groot, F.; Kotani, A. Core Level Spectroscopy of Solids. *Advances in Condensed Matter Science*; CRC: Boca Raton, FL, USA, 2008.
(28) De Groot, F. M. F.; Fuggle, J. C.; Thole, B. T.; Sawatzky, G. A. *Phys. Rev. B* **1990**, *42*, 5459–5468.
(29) Stavitski, E.; de Groot, F. M. F. *Micron* **2010**, *41*, 687–694.
(30) Cowan, R. D. *the Theory of Atomic Structure and Spectra*; University of California Press: Berkeley, CA, USA, 1981.
(31) Kroll, T.; Aristov, V. Y.; Molodtsova, V.; Ossipyan, Y. A.; Vyalikh, D. V.; Büchner, B.; Knupfer, M. *J. Phys. Chem. A* **2009**, *113*, 8917–8922.
(32) Neese, F. *The ORCA program system.* Wiley Interdisciplinary Reviews, Computational Molecular Science; Wiley: New York, 2011.
(33) Neese, F.; Petrenko, T.; Ganyushin, D.; Olbrich, G. *Coord. Chem. Rev.* **2007**, *251*, 288–327.
(34) Pantazis, D. A.; Chen, X. -.; Landis, C. R.; Neese, F. *J. Chem. Theory Comput.* **2008**, *4*, 908–919.
(35) Eichkorn, K.; Treutler, O.; Öhm, H.; Häser, M.; Ahlrichs, R. *Chem. Phys. Lett.* **1995**, *240*, 283–289.
(36) Eichkorn, K.; Weigend, F.; Treutler, O.; Ahlrichs, R. *Theor. Chem. Acc.* **1997**, *97*, 119–124.
(37) Petrenko, T.; Neese, F. *J. Chem. Phys.* **2007**, *127*, 164319.
(38) Petrenko, T.; Kossmann, S.; Neese, F. *J. Chem. Phys.* **2011**, *134*, No. 054116.
(39) DeBeer George, S.; Petrenko, T.; Neese, F. *J. Phys. Chem. A* **2008**, *112*, 12936–12943.
(40) DeBeer George, S.; Petrenko, T.; Neese, F. *Inorg. Chim. Acta* **2008**, *361*, 965–972.
(41) George, S. D.; Neese, F. *Inorg. Chem.* **2010**, *49*, 1849–1853.
(42) Neese, F. *Inorg. Chim. Acta* **2002**, *337*, 181–192.
(43) de Groot, F. M. F.; Elec., J. *Spec. Rel. Phenom.* **1994**, *67*, 529–622.
(44) de Groot, F. *Coord. Chem. Rev.* **2005**, *249*, 31–63.
(45) Cook, P. L.; Liu, X.; Yang, W.; Himpsel, F. J. *J. Chem. Phys.* **2009**, *131*, 194701.
(46) Sabelli, N. H.; Melendres, C. A. *J. Phys. Chem.* **1982**, *86*, 4342–4346.